PHILOSOPHICAL TRANSACTIONS OF THE ROYAL SOCIETY A

Phil. Trans. R. Soc. A (2008) **366**, 33–45
doi:10.1098/rsta.2007.2137
Published online 7 September 2007

Stark spectroscopy of mixed-valence systems

By Lisa N. Silverman, Pakorn Kanchanawong, Thomas P. Treynor and Steven G. Boxer*

Department of Chemistry, Stanford University, Stanford, CA 94305-5080, USA

Many mixed-valence systems involve two or more states with different electric dipole moments whose magnitudes depend upon the charge transfer distance and the degree of delocalization; these systems can be interconverted by excitation of an intervalence charge transfer transition. Stark spectroscopy involves the interaction between the change in dipole moment of a transition and an electric field, so the Stark spectra of mixed-valence systems are expected to provide quantitative information on the degree of delocalization. In limiting cases, a classical Stark analysis can be used, but in intermediate cases the analysis is much more complex because the field affects not only the band position but also the intrinsic bandshape. Such non-classical Stark effects lead to widely different bandshapes. Several examples of both classes are discussed. Because electric fields are applied to immobilized samples, complications arise from inhomogeneous broadening, along with other effects that limit our ability to extract unique parameters in some cases. In the case of the radical cation of the special pair in photosynthetic reaction centres, where the mixed-valence system is in a very complex but structurally well-defined environment, a detailed analysis can be performed.

Keywords: Stark spectroscopy; reaction centre; mixed valence; intervalence; charge transfer; Creutz–Taube ion

1. Introduction

The effects of an electric field on the absorption (or emission) from a molecule are known collectively as the Stark effect. In many cases, the applied electric field, $\boldsymbol{F}$, can be treated as a simple perturbation to an absorber's transition dipole moment, $\boldsymbol{m}$, and peak position, $\bar{\nu}_{\max}$, but not to its population or its bandshape. These are called classical Stark effects. In the following, we consider only cases in which the ensemble of absorbers is isotropic and the distribution of orientations is unaffected by the field, for example when the sample is in a frozen glass or immobilized in a polymer film, as these are the simplest to work with. So long as the field perturbations to the individual transitions are small when compared with their bandwidths and intensities, the absorption Stark spectrum $\Delta A = A(\boldsymbol{F} \neq 0) - A(\boldsymbol{F} = 0)$ can be expressed as a sum of the zeroth, first and

* Author for correspondence (sboxer@stanford.edu).

One contribution of 15 to a Discussion Meeting Issue 'Mixed valency'.

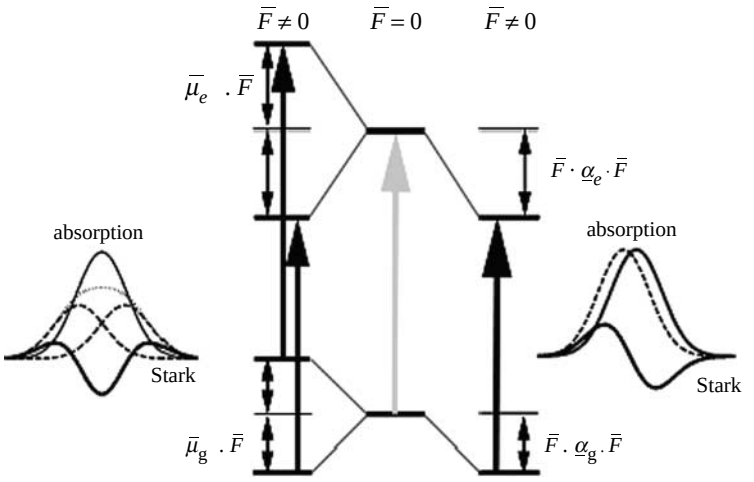

Figure 1. Effect of an external electric field on the bandshape of an absorber according to the classical model.

second $\bar{\nu}$-weighted derivatives of the absorption spectrum

$$\Delta A(\boldsymbol{F}, \chi) = f^2 \boldsymbol{F}^2 \left\{ A_\chi \cdot A(\bar{\nu}) + \frac{B_\chi}{15hc} \bar{\nu} \frac{\partial}{\partial \bar{\nu}} \left(\frac{A(\bar{\nu})}{\bar{\nu}} \right) + \frac{C_\chi}{30h^2c^2} \bar{\nu} \frac{\partial^2}{\partial \bar{\nu}^2} \left(\frac{A(\bar{\nu})}{\bar{\nu}} \right) \right\}. \quad (1.1)$$

In this equation h is Planck's constant and c is the speed of light; χ is the experimental angle between $\boldsymbol{F}$ and the polarization of the probing light field; and f is a scalar approximation to the local field correction tensor. This tensor is intended to account for a possible difference between $\boldsymbol{F}$, the externally applied field, and $\boldsymbol{F}_{\mathrm{int}}$, the internal field at the position of a chromophore $\boldsymbol{F}_{\mathrm{int}} = f \cdot \boldsymbol{F}$. It is generally believed that, for most frozen organic or aqueous glasses, the value of f is between 1.0 and 1.3. The full expressions for the coefficients A_χ, B_χ and C_χ have been defined elsewhere (Bublitz & Boxer 1997); they provide information on the transition polarizability, $\underline{A}$, and transition hyperpolarizability, $\underline{B}$, the difference polarizability, $\Delta\alpha$, and the difference dipole moment, $\Delta\boldsymbol{\mu}$ (figure 1).

The classical model has been used to analyse the intervalence band (IVB) Stark effect for a number of mixed-valence complexes (MVCs). However, there are instances in which the underlying assumptions that the electric field does not affect the population or the bandshape of a transition do not hold. Intervalence transitions in MVCs arise from the vibronic coupling between two charge-localized electronic states, ψ_{L} and ψ_{R}, causing a breakdown of the Born–Oppenheimer approximation for the eigenstates of MVCs between the limits of weak and strong mixing of ψ_{L} and ψ_{R}. The adiabatic electronic charge transfer states

$$\psi_1(q) = c_1(q)\psi_{\mathrm{L}} + c_2(q)\psi_{\mathrm{R}} \quad \text{and} \quad \psi_2(q) = -c_2(q)\psi_{\mathrm{L}} + c_1(q)\psi_{\mathrm{R}} \quad (1.2)$$

and the difference dipole moment between them, $\Delta\mu_{\mathrm{CT}}$, thus depend on the nuclear configuration q. The Born–Oppenheimer violation is necessarily ignored when the IVB is treated with a purely electronic coupling model (such as the classical sum of derivatives model, equation (1.1)) instead of a vibronic coupling model. The electronic coupling models of IVB absorption can also fail to recognize that some MVCs have adiabatic groundstate potential energy surfaces that are double welled, giving rise to two distinct, though generally overlapping, absorption

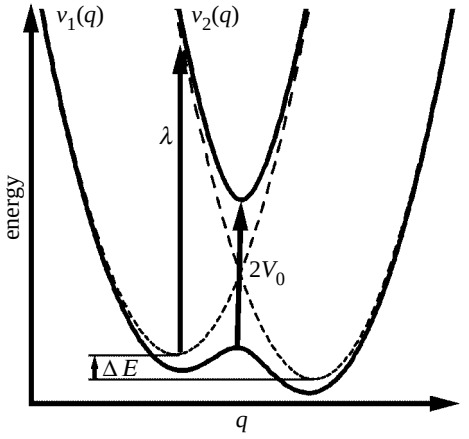

Figure 2. Electron transfer parameters describing a mixed-valence system. Dashed lines are adiabatic localized charge transfer states and solid lines are adiabatic charge transfer states.

spectra. Thus, a failure to recognize the intrinsically vibronic nature of the coupling between ψ_L and ψ_R could lead to a misinterpretation of the results of a classical Stark analysis of the IVB for two reasons: first, on account of the Born–Oppenheimer violation, the adiabatic electronic states of many MVCs have q-dependent dipole moments, so it is not clear what physical property the fit value of $\Delta\mu$ from a classical Stark analysis (equation (1.1)) might represent; second, there are some cases in which the applied electric field will effect a population transfer between two nearly degenerate wells, thus violating an assumption of the classical model.

In order to account for the vibronic coupling in MVCs, Treynor and Boxer developed a general model for analysing IVB Stark effects based on Marcus–Hush theory, which we call the 'non-classical' model (Treynor & Boxer 2004). In this model, the standard electron transfer parameters of vibronic coupling, V_0, driving force, ΔE, coupled vibrational mode, $\bar{\nu}_{anti}$ or $\bar{\nu}_{sym}$, and reorganization energy, λ_{anti} or λ_{sym}, denoting an antisymmetric or a symmetric mode and reorganization energy, respectively (figure 2), are employed to calculate the bandshape of the IVB in the presence and the absence of an applied electric field. Symmetric modes are expected to be relevant only for highly coupled MVCs; only antisymmetric modes are used for the systems described in this paper. The application of an electric field affects the driving force ΔE of different orientational subpopulations to a varying degree. In the Franck–Condon picture, this variation in ΔE gives rise to different intrinsic bandshapes for different orientational subpopulations (assuming that the electronic coupling and reorganization energy are not affected by the electric field). Therefore, in an isotropic distribution of MVCs in an electric field, a variety of bandshapes will be present, which must be calculated independently in order to determine the orientationally averaged Stark effect.

There are several benefits to using the non-classical over the classical model. First, the bandshape and population are allowed to change in response to the electric field, providing a more accurate description for what occurs in most class II/III systems. In addition, the non-classical model is much more information-rich, providing two different, but related, ways to analyse the degree of

localization in an MVC. The first, per cent localization, $\%L$, is a graded description of the degree of mixing between the charge-localized states. This quantity can be estimated from the probability density of ψ_{L} in $\psi_1(q)$ at $q_{\min}$

$$\%L = |c_1(q_{\min})|^2 \times 100. \tag{1.3}$$

A value of 0 or 100 indicates no mixing of ψ_{L} and ψ_{R}, while a value of 50 indicates complete mixing. All values in between are possible. This description is independent of temperature, since it involves only the mixing of the states and says nothing about their populations. The second method involves an analysis of the potential energy surfaces of MVCs. The electron transfer parameters obtained from the fits can be used to generate the adiabatic surfaces $V_1(q)$ and $V_2(q)$ corresponding to $\psi_1(q)$ and $\psi_2(q)$ given by

$$V_1(q) = \frac{\bar{\nu}_{\mathrm{anti}}}{2}(q^2 + \delta^2) + \frac{\Delta E}{2} - \frac{1}{2}[(2\delta q - \Delta E)^2 + 4V_0^2]^{1/2} \quad \text{and} \tag{1.4}$$

$$V_2(q) = \frac{\bar{\nu}_{\mathrm{anti}}}{2}(q^2 + \delta^2) + \frac{\Delta E}{2} + \frac{1}{2}[(2\delta q - \Delta E)^2 + 4V_0^2]^{1/2}, \tag{1.5}$$

where δ is a function of λ_{anti} and $\bar{\nu}_{\mathrm{anti}}$ (figure 2). A more general treatment that includes symmetric modes has been described elsewhere (Treynor & Boxer 2004). Insight into the behaviour of the MVC can be gained by applying the Franck–Condon principle to transitions between these surfaces. Although this principle is ultimately derived from the Born–Oppenheimer approximation which, as discussed above, does not hold for many MVCs, this approach leads to useful qualitative estimates of the behaviour of MVCs. From the adiabatic surfaces, one can directly determine whether the molecule has one or two groundstate minima. A simple criterion for identifying the localized-to-delocalized transition was proposed (equation (1.6)), in which there is only a single minimum on the groundstate potential energy surface when the following inequality holds:

$$\frac{4V_0^2}{(\Delta E + \lambda_{\mathrm{anti}})^2 + 4V_0^2} \geq \frac{1}{2}. \tag{1.6}$$

Also, if there are two minima, the barrier to thermal electron transfer can be determined approximately, thus providing a prediction of the sensitivity of the transition to temperature and electric field. This description of the MVC can account for the populations of the states, since the electrons or holes can be described as localized if they are lower in energy and delocalized if they are higher in energy than the thermal barrier.

Within the limits of very strong and very weak couplings (provided there is no effect of field on the populations of the charge-localized states), the classical and non-classical methods of analysis provide an interchangeable description of the states involved. In addition, for many intermediate MVCs, the values of $\Delta\mu$ obtained from the classical model are predicted to be similar to those of $\Delta\mu_{\mathrm{CT}}$ obtained from the non-classical model. However, the non-classical analysis yields more information and can avoid incorrect assumptions, and it is the correct description for the most interesting cases that fall between the limits of strong and weak couplings.

Figure 3. MVCs that have been probed by Stark spectroscopy.

2. Experimental

Details of the methods used to obtain Stark spectra have been described elsewhere (Bublitz & Boxer 1997). The sample must be thin enough to achieve a high field with a high-voltage power supply without breakdown on a frozen glass (sample thicknesses are typically tens of micrometres with applied voltages up to several thousand volts, giving fields of up to 1 MV cm^{-1}). In order to achieve this, a special cryostat has been designed so that the sample can be immersed in liquid nitrogen for efficient cooling but without optical interference; thus most data are obtained at approximately 77 K and it is difficult to vary the temperature (Andrews & Boxer 2000).

For all spectra shown in this paper (and most from our laboratory), the absorption has been scaled to a value of 1 at the absorption maximum, and Stark spectra have been scaled to the absorption spectra and to an external electric field $\boldsymbol{F}$ of 1 MV cm^{-1} (all Stark spectra observed to date depend quadratically on $\boldsymbol{F}$). For all values of $\Delta\mu$ and $\Delta\mu_{CT}$, the local field correction factor f is assumed to be 1.

3. Results and discussion

In the following, we consider the analysis of a series of systems shown in figure 3, comparing the classical sums of derivative method (equation (1.1)) with the more sophisticated non-classical Stark model.

(*a*) *Creutz–Taube ion*

The classic example of a mixed-valence compound with intermediate behaviour is the Creutz–Taube ion, **1**, whose Stark spectrum is shown in figure 4 (Oh *et al.* 1991). Qualitatively, the Stark spectrum does not have a dominant second-derivative bandshape, rather it looks like a negative zeroth derivative for all but the highest energy portion of the band, indicating that the principal effect of the electric field is a loss of intensity of the IVB. The absence of a predominant second-derivative component suggests that $\Delta\mu$ is small. The band can be well fitted by the classical model at wavenumbers below 6500 cm^{-1}, giving best-fit values for $\Delta\mu$ of 0.8 debye if only the lower wavenumber portion of the band is fitted, and 2.0 debye if the entire band is fitted up to 12 000 cm^{-1}. In either case,

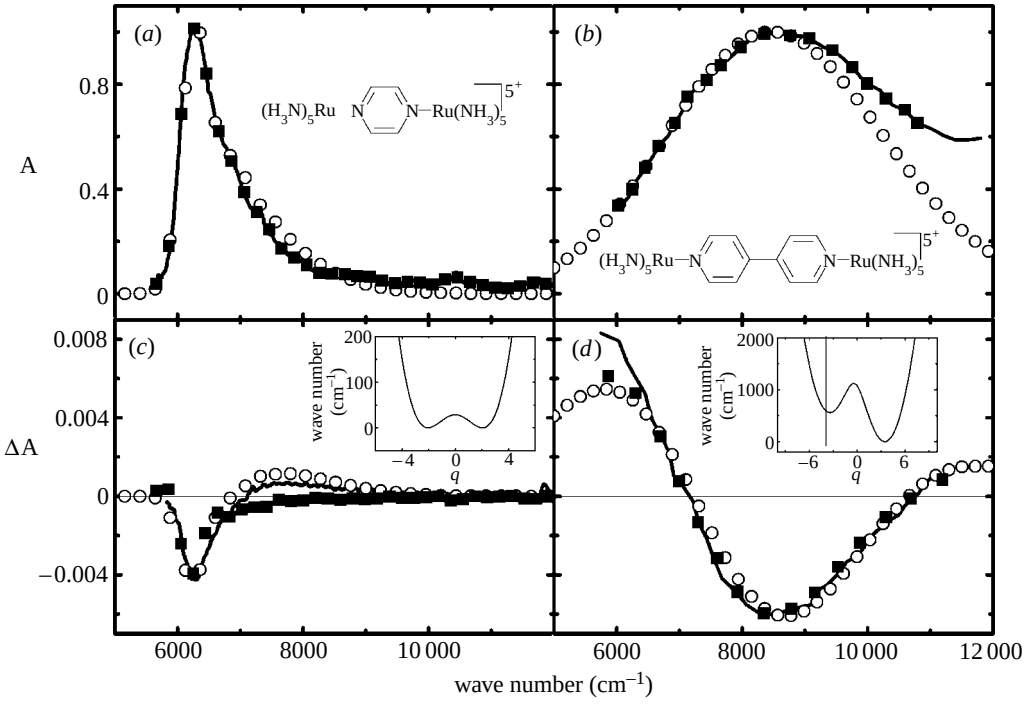

Figure 4. (*a*,*b*) Absorption and (*c*,*d*) Stark spectra of **1** and **2** in 1 : 1 water/glycerol at 77 K; counter ions are $(C_7H_7SO_3^-)_5$ and $(Br^-)_5$, respectively. Data (solid lines) fit to the classical model (filled squares) and the non-classical model (open circles) are shown, along with the groundstate potential energy surfaces derived from the non-classical model (inset). Fit parameters are listed in table 1.

$\Delta\mu$ is much smaller than the predicted value of 33 debye if a full charge were transferred between the centres of the ruthenium atoms, suggesting that the Creutz–Taube ion is close to the delocalized limit.

The non-classical model provides a qualitatively similar but more detailed description of the intervalence transition. The value of $\Delta\mu_{CT}$ is 3.4 debye from the non-classical model, which is similar to that obtained from the classical model and still consistent with a high degree of delocalization. If we apply the criteria for delocalization shown in equation (1.6), the Creutz–Taube ion does not fall into class III. The groundstate potential energy surface for **1** has two distinct minima with a barrier to thermal electron transfer of 30 cm^{-1}. Therefore, we can conclude that the Creutz–Taube ion is not strictly class III, although the holes are effectively delocalized at temperatures above 45 K. Looking purely at the mixing between the charge-localized states, $\%L$ is 75, intermediate between strong and weak mixing.

(*b*) *Longer bridging ligands*

We can compare the results for the Creutz–Taube ion with those for the similar compound **2**, in which the bridging pyrazine ligand has been replaced by a 4,4′-bipyridyl ligand (Oh *et al.* 1991). The longer bridge is expected to reduce significantly the coupling between the ruthenium centres, leading to a much more localized mixed-valence compound. Hush theory analysis of the broad, weak IVB suggests

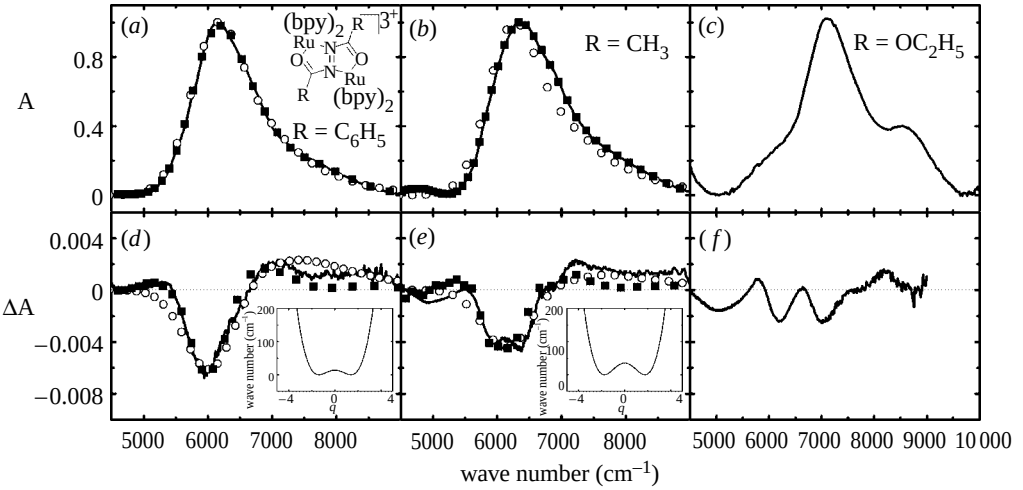

Figure 5. (*a–c*) Absorption and (*d–f*) Stark spectra of **3**, **4** and **5** in 1 : 1 propionitrile/butyronitrile at 77 K. Data (solid lines) fit to the classical model (filled squares) and the non-classical model (open circles) are shown, along with the groundstate potential energy surfaces derived from the non-classical model (inset). Fit parameters are listed in table 1.

that the hole in **2** is 99.8% localized on one ruthenium centre (Oh *et al.* 1991). At first glance, the Stark spectrum of **2** is similar in magnitude to that of **1** (figure 4). However, in contrast to **1**, the Stark bandshape of **2** is dominated by the second-derivative component. The classical analysis shows sizable contributions from the zeroth and first derivatives, but most of the Stark effect is due to the interaction of the external electric field with the difference dipole moment of the molecule. The classical model, which is expected to be valid for strongly localized MVCs, gives a value of $\Delta\mu$ of 28 debye. This is still only 52% of the 54 debye expected for transfer of a full charge between the ruthenium centres, but it is an order of magnitude larger than the $\Delta\mu$ of **1**, representing a significantly more localized situation.

The non-classical model gives a similar value of $\Delta\mu_{CT}$ of 24 debye, however other fit parameters are revealing of interesting behaviour in this compound. In particular, the Stark spectrum can only be fitted by using a non-zero value of ΔE. Although this is a symmetric molecule, the redox asymmetry due to the strong localization could lead to differential interactions with solvent molecules and/or counter ions, and thus transient symmetry breaking which may get trapped when rapidly frozen. $\%L$ for **2** is 95, confirming that there is little mixing between the charge-localized states, and the thermal barrier between the two groundstate energy minima is 1100 cm^{-1}. In contrast to the Creutz–Taube ion, and despite the smaller than expected value of $\Delta\mu_{CT}$, **2** is solidly in class II.

(*c*) *Tunable bridging ligands*

Another case that appears to fall on the class II/III borderline is the series of diruthenium compounds $[\{Ru_2(bpy)_2\}_2(adc\text{-}R)](PF_6)_2(Br_3)$ (adc-R = azodicarbonyl ligand O=C–(R)–N=N–C–(R)=O, bpy = 2,2′-bipyridyl; Kaim & Kasack 1990), in which the bridging ligand can be finely tuned by changing the identity of the group R (figure 3). Following the work of Kaim *et al.*, we have prepared the

compounds in which R= $-OCH_3$, $-OC_2H_5$, $-CH_3$, $-C_6H_5$, $-C_6H_4COOH$ and $-C_6H_3F_2$, all of which have very intense, solvent-independent IVBs in the 6000–7000 cm^{-1} range and large comproportionation constants, indicative of delocalization (Kasack *et al.* 1995). Conversely, XPS spectra show two sets of ruthenium binding energies, consistent with a more localized description, though this technique has been criticized for its potential to bias a mixed valence complex towards localization (Citrin 1973; Citrin & Ginsberg 1981). EPR data show increasing g-anisotropy as the electron accepting character of R increases. Since MVCs involving Ru(III) are expected to show large g-anisotropies due to spin-orbit coupling (Stebler *et al.* 1984; Khan *et al.* 1990), this trend has been interpreted as a shift from a bridge-centred to a metal-centred unpaired electron (Kasack *et al.* 1995).

The compounds in which R=aryl or alkyl have near-IR absorption bands with similar bandshapes to that of the Creutz–Taube ion. Absorption and Stark spectra for **3** and **4**, along with fits to both the classical and non-classical models, are shown in figure 5. Both the models are able to fit the spectra well and give similar values for $\Delta\mu$ and $\Delta\mu_{CT}$ (5.6 debye for **3** and 4.0 debye for **4**). For both compounds, the values of $\Delta\mu_{CT}$ are significantly smaller than one would predict from the Ru–Ru distance. We obtained a crystal structure of **3** in the mixed-valence form, and it indicates that the Ru–Ru distance is 5 Å, which would give $\Delta\mu_{CT}=24$ debye. Besides the small values of $\Delta\mu_{CT}$, analysis of the electronic parameters obtained from the non-classical model indicate that $\%L$ is 74 and 76 for **3** and **4**, respectively, indicative of intermediate mixing of the charge-localized states. The groundstate potential energy surface shows two distinct minima, but the barrier to thermal electron transfer is less than 50 cm^{-1} in both cases, indicating that at extremely low temperatures the electron is localized, but that it is effectively delocalized above approximately 50 K.

In contrast, the compounds in which R=alkoxy (i.e. **5**) do not give such clear results. The spectra are much more complex and cannot be fitted well with either model (figure 5). There are several possible origins for the more complex bandshape. One possibility is that spin-orbit coupling is a more dominant factor in these compounds than in their alkyl or aryl counterparts. The presence of multiple overlapping bands from different vibronic states is a difficult problem for any bandshape analysis, since the different states would give rise to different electron transfer parameters. Since there is no standard bandshape for intervalence absorption bands or their corresponding Stark effects, there is no reliable method to parse the spectra into individual components. The dominance of spin-orbit coupling in the bandshapes of many ruthenium-based MVCs makes quantitative analysis of the Stark spectra of such compounds very difficult. Also, there may be more vibrational modes that are significantly coupled to the charge transfer. The non-classical model allows for the inclusion of up to two modes at present. A larger number of modes could be included, but the already large number of adjustable parameters would increase, requiring additional experiments like resonance Raman spectroscopy to be done in order to limit some of the variables.

(*d*) *Osmium complexes*

The compound *trans, trans*-$\{[(tpy)(Cl)_2Os]_2(N_2)\}(PF_6)$, **6**, is another example of interesting mixed-valence behaviour. Because osmium has a large spin-orbit coupling, such complexes are expected to have three distinct IVBs in the

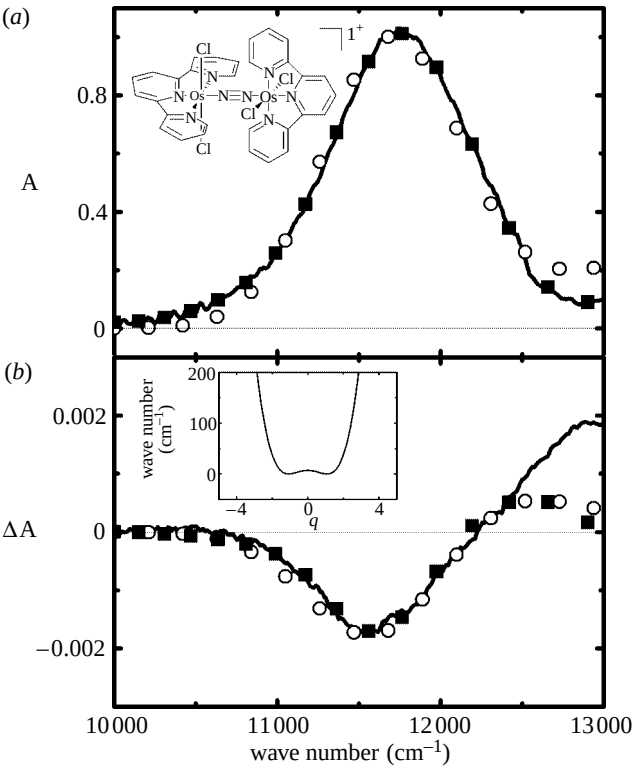

Figure 6. (*a*) Absorption and (*b*) Stark spectra of **6** in 1 : 1 propionitrile/butyronitrile at 77 K. Data (solid lines) fit to the classical model (filled squares) and the non-classical model (open circles) are shown, along with the groundstate potential energy surfaces derived from the non-classical model (inset). Fit parameters are listed in table 1.

absorption spectrum. The lowest energy IVB has been assigned to a weak transition at 5200 cm^{-1} (Demadis *et al.* 1999). This band overlaps significantly with another band that has been assigned to a $d\pi$–$d\pi$ interconfigurational transition, making it difficult to isolate and analyse by Stark spectroscopy. The remaining two IVBs are very close in wavenumber, comprising what appears as a single band at 11 500 cm^{-1}. This is the band that we will focus on. This 11 500 cm^{-1} band is intense and narrow, indicative of a high degree of delocalization. In contrast, there is an intense band at 2007 cm^{-1} corresponding to the N=N stretching mode (Demadis *et al.* 1999), suggesting that there must be some redox asymmetry in order to make this otherwise forbidden symmetric mode allowable. This mode is present both in fluid solution at room temperature and in a frozen glass at 77 K.

The Stark spectrum of the 11 500 cm^{-1} band is dominated by the second derivative of the absorption (figure 6). The classical model provides a good fit except at the extreme blue end of the spectrum, which is likely to be due to an overlap of the IVB with adjacent metal–ligand charge transfer bands, and gives a value of $\Delta\mu = 2.1$ debye. The non-classical model is also able to fit all but the highest energy part of the band, giving a value of 4.5 debye for $\Delta\mu_{CT}$. This is much less than the 24 debye expected for full Os–Os hole transfer, and it suggests

that the holes are localized more on the bridging nitrogen atoms. Calculation of $\%L$ from the non-classical model gives a value of 73, and the groundstate potential energy surface indicates two minima with a thermal barrier of less than $10\ \mathrm{cm}^{-1}$, putting **6** in class II/III, with a bias towards class III.

(*e*) *The special pair cation in photosynthetic reaction centres*

The reaction centre (RC) from photosynthetic bacteria is the site of the initial light-driven electron transfer processes in photosynthesis. Stark spectroscopy has proven to be a rich tool for studying the RC and many new types of Stark effects were first discovered in this system. The primary electron donor is a pair of bacteriochlorophyll molecules denoted P and often called the special pair; a view of P including several key nearby amino acid residues is shown in figure 3. P^* transfers an electron to B_L and H_L within a few ps, leaving the cation radical P^+. The hole on P^+ has been characterized in great detail by EPR and ENDOR, and different degrees of delocalization are observed when amino acids that interact with P are altered, especially those that remove or add hydrogen bonds to carbonyl groups on the special pair.

Breton discovered an intense mid-IR electronic absorption band associated with P^+, and this has been shown to be an intervalence charge transfer band (Breton *et al.* 1992). The P^+ IVB is very broad and overlaps significantly with intense solvent and protein vibrational modes. Fortunately, the rapid photochemical cycle of the RC allows us to generate P^+ reversibly by visible actinic excitation and thus take the absorption spectra as the light-induced difference spectra (ΔA) and the Stark spectra as the light-induced field-induced double-difference spectra ($\Delta\Delta$A). The stability of the FTIR also enables us to signal average over an extended period and, by using an IR detector with good linearity (InSb), the difference technique is expected to give accurate bandshape information. Further, the difference spectra readily reveal the highly structured phase-phonon absorption bands that correspond to vibrational modes coupled with intervalence charge transfer (Reimers & Hush 2003).

We have shown that the analysis of the Stark spectra of wild-type P^+ using the classical model gives a relatively small value of $\Delta\mu$ of 8.2 debye (Treynor *et al.* 2003). On the other hand, using the non-classical model, a value of $\Delta\mu_{CT}$ of 32 debye was obtained, which is in better agreement with the structure and the extent of localization measured by ENDOR/TRIPLE experiments (Treynor *et al.* 2003). Subsequently, we measured the Stark spectra of the hydrogen-bond mutant RCs and observed significant variation in bandshape and magnitude among the mutants as shown in figure 7 (Kanchanawong *et al.* 2006). These mutations alter the degree of localization by altering the energy asymmetry of P^+. For example, in wild-type RC, P^+ is intermediately asymmetric; the L131LH mutation renders P^+ nearly symmetric, the M160LH mutation makes P^+ highly asymmetric and localized, while the M160LH/L131LH double mutation restores wild-type-like extent of localization. We compared the analyses of the Stark spectra using both a minimal form of the non-classical Stark model (two electronic states, one coupled vibrational mode: 2/1 A&S) and a more extensive model that includes four electronic states and 70 vibrational modes (4/70 A&S). The four-state–70-mode model was developed by Reimers & Hush (2003) to account quantitatively for the shoulder on the main IVB, treated

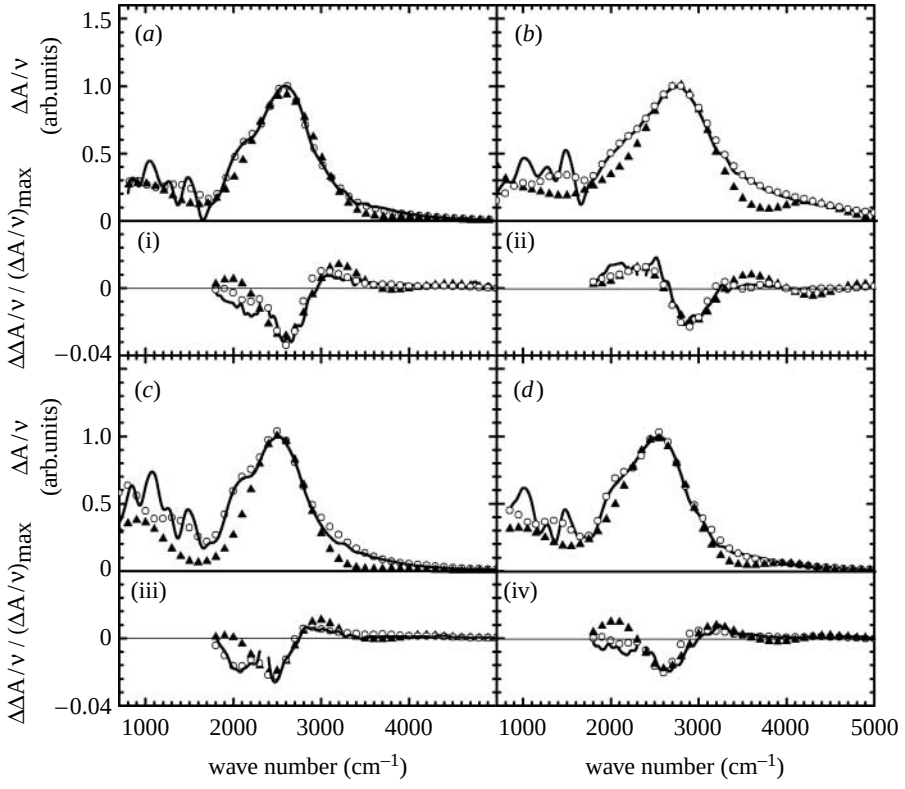

Figure 7. (*a–d*) Absorption, WT, M160LH, L131LH and M160LH/L131LH, respectively, and (i–iv) Stark spectra of wild-type and mutant RCs as dehydrated protein films at 77 K. Data (lines), fits to the 2-state-1-mode non-classical model (triangles), and fits to the 4-state-70-mode non-classical model (circles) are shown.

here as the SHOMO to HOMO (Reimers *et al.* 2003) transition, as well as the phase-phonon bands in which the multitude of peaks in the spectra indicate involvement of multiple vibrational modes. Simulations from both the models, as shown in figure 7, are in good agreement with the observed spectra. The electron transfer parameters thus obtained also agree well with results from previous studies that extract the parameters by relating the electrochemical potential and charge localization for 22 mutant RCs (Hughes *et al.* 2001). Since we examine individual mutants independently and determine the electron transfer parameters simultaneously, the specific effects of the mutations are elucidated. Among the major and unexpected changes are the values of the electronic coupling, which are appreciably reduced in the M160LH mutant, and $\Delta\mu_{CT}$, which ranges from 32–35 debye for wild-type to 21 debye for M160LH.

The example of the P^+ series demonstrates that, in a case where properties of the system allow the intervalence absorption and Stark spectra to be measured accurately, the non-classical Stark model can be applied successfully over a wide range of parameters and gives results consistent with estimates independently arrived at by the analysis of other observables. While the highly complex protein environment may at first suggest a potentially complicated behaviour, it appears that the structural specificity of the protein environment is beneficial in

Table 1. Electron transfer parameters from the non-classical model and comparison with $\Delta\mu$ from the classical model.

	λ_{anti} (cm^{-1})	V_0 (cm^{-1})	ΔE (cm^{-1})	$\bar{\nu}_{\text{anti}}$ (cm^{-1})	FWHM (cm^{-1})	$\%L$	$\Delta\mu_{\text{CT}}$ (debye, non-classical)	$\Delta\mu$ (debye, classical)
1	7000	3050	0	200	500	74	3.4	2.0
2	8200	1500	600	300	2000	95	24	28
3	6500	2950	0	300	950	76	5.6	5.6
4	7000	3000	0	300	900	72	4.0	4.0
5	—	—	—	—	—	—	—	—
6	12 000	5700	0	500	900	73	4.5	2.1

constraining the geometry and maintaining a similar 'solvent' environment for the MVC. Hence, the intended perturbation to the energy asymmetry of P^+ works largely as intended, with no major structural rearrangements that affect other key parameters, and this is preserved even when the sample is frozen (nearly all the early electron transfer events in the RC occur efficiently at low temperature and the X-ray structure was determined at 77 K). Even so, it must be noted that the effect of different mutations on other electron transfer parameters are not negligible, as indicated by the fit parameters; in particular the changes in the values of the electronic coupling and $\Delta\mu_{\text{CT}}$ for the M160LH mutation are quite substantial (Kanchanawong *et al.* 2006). In simpler solvents with no scaffolding effect of the protein, it is conceivable that the structural rearrangement of MVCs will be more common and extensive.

In the simulation for non-classical Stark model, we account for the effect of inhomogeneous broadening on the spectra using a Gaussian with a finite width for all the transitions. While this is a widely used approximation, in the case of mixed-valence systems it is uncertain whether the symmetric Gaussian is an appropriate choice. The effect of local heterogeneity can potentially result in asymmetric broadening of the spectra; for instance, as described earlier, when a symmetric mixed-valence system becomes asymmetric, its spectra are expected to shift towards higher frequency and to broaden. Thus, it is probable that the fit quality of the simulated spectra is affected by errors in simulating the inhomogeneous broadening envelope (table 1).

We would like to thank Dr Reginaldo C. Rocha in Andrew P. Shreve's laboratory at Los Alamos National Laboratory for providing us with the dinuclear osmium compound. This work was supported in part by the NSF Biophysics Program.

References

Andrews, S. S. & Boxer, S. G. 2000 A liquid nitrogen immersion cryostat for optical measurements. *Rev. Sci. Inst.* **71**, 3567–3569. (doi:10.1063/1.1287343)

Breton, J., Nabedryk, E. & Parson, W. W. 1992 A new infrared electronic transition of the oxidized primary electron donor in bacterial reaction centers: a way to assess resonance interactions between the bacteriochlorophylls. *Biochemistry* **31**, 7503–7510. (doi:10.1021/bi00148a010)

Bublitz, G. U. & Boxer, S. G. 1997 Stark spectroscopy: applications in chemistry, biology and materials science. *Annu. Rev. Phys. Chem.* **48**, 213–242. (doi:10.1146/annurev.physchem.48.1.213)

Citrin, P. H. 1973 Direct evidence for charge localization in pyrazine-bridged mixed-valence ruthenium complexes. *J. Am. Chem. Soc.* **95**, 6472–6473. (doi:10.1021/ja00800a064)

Citrin, P. H. & Ginsberg, A. P. 1981 X-ray photoemission from the Creutz–Taube mixed valence complex: a reassessment. *J. Am. Chem. Soc.* **103**, 3673–3679. (doi:10.1021/ja00403a011)

Demadis, K. D., El-Samanody, E.-S., Coia, G. M. & Meyer, T. J. 1999 OsIII(N2)OsII complexes at the localized-to-delocalized, mixed-valence transition. *J. Am. Chem. Soc.* **121**, 535–544. (doi:10.1021/ja982802o)

Hughes, J. M., Hutter, M. C., Reimers, J. R. & Hush, N. S. 2001 Modeling the bacterial photosynthetic reaction center. 4. The structural, electrochemical, and hydrogen-bonding properties of 22 mutants of *Rhodobacter sphaeroides*. *J. Am. Chem. Soc.* **123**, 8550–8563. (doi:10.1021/ja0035710)

Kaim, W. & Kasack, V. 1990 Stability rules for d5/d6 mixed-valent dimers. Effects from the donor/acceptor capability of the metal (ruthenium vs osmium) and from the occupancy of the mediating ligand orbital (LUMO vs HOMO). *Inorg. Chem.* **29**, 4696–4699. (doi:10.1021/ic00348a022)

Kanchanawong, P., Dahlbom, M. G., Treynor, T. P., Reimers, J. R., Hush, N. S. & Boxer, S. G. 2006 Charge delocalization in the special-pair radical cation of mutant reaction centers of *Rhodobacter sphaeroides* from stark spectra and nonadiabatic spectral simulations. *J. Phys. Chem. B* **110**, 18 688–18 702. (doi:10.1021/jp0623894)

Kasack, V., Kaim, W., Binder, H., Jordanov, J. & Roth, E. 1995 When is an odd-electron dinuclear complex a mixed-valent species? Tuning of ligand-to-metal spin shifts in diruthenium(III,II) complexes of noninnocent bridging ligands OC(R)NNC(R)O. *Inorg. Chem.* **34**, 1924–1933. (doi:10.1021/ic00111a045)

Khan, M. M. T., Srinivas, D., Kureshy, R. I. & Khan, N. H. 1990 Synthesis, characterization, and EPR studies of stable ruthenium(III) Schiff base chloro and carbonyl complexes. *Inorg. Chem.* **29**, 2320–2326. (doi:10.1021/ic00337a026)

Oh, D. H., Sano, M. & Boxer, S. G. 1991 Electroabsorption (Stark effect) spectroscopy of mono- and biruthenium charge-transfer complexes: measurements of changes in dipole moments and other electrooptic properties. *J. Am. Chem. Soc.* **113**, 6880–6890. (doi:10.1021/ja00018a026)

Reimers, J. R. & Hush, N. S. 2003 Modeling the bacterial photosynthetic reaction center. VII. Full simulation of the intervalence hole-transfer absorption spectrum of the special-pair radical cation. *J. Chem. Phys.* **119**, 3262–3277. (doi:10.1063/1.1589742)

Reimers, J. R., Shapley, W. A. & Hush, N. S. 2003 Modelling the bacterial photosynthetic reaction center. V. Assignment of the electronic transition observed at 2200 cm^{-1} in the special-pair radical-cation as a second-highest occupied molecular orbital to highest occupied molecular orbital transition. *J. Chem. Phys.* **119**, 3240–3248. (doi:10.1063/1.1569909)

Stebler, A., Ammeter, J. H., Furholz, U. & Ludi, A. 1984 The Creutz–Taube complex revisited: a single-crystal EPR study. *Inorg. Chem.* **23**, 2764–2767. (doi:10.1021/ic00186a010)

Treynor, T. P. & Boxer, S. G. 2004 A theory of intervalence band stark effects. *J. Phys. Chem. A* **108**, 1764–1778. (doi:10.1021/jp035890u)

Treynor, T. P., Andrews, S. S. & Boxer, S. G. 2003 Intervalence band stark effect of the special pair radical cation in bacterial photosynthetic reaction centers. *J. Phys. Chem. B* **107**, 11 230–11 239. (doi:10.1021/jp035039f)